Study of the 6Li(n,)3H reaction via the 2H quasi-free break-up

M Gulino, C Spitaleri, S Cherubini, V Crucillà, M La Cognata, L Lamia, R G Pizzone, S Romano, M L Sergi, A Tumino, et al.

Study of the $^6Li(n,\alpha)^3H$ reaction via the ^2H Quasi-Free Break-up

M. Gulino, C. Spitaleri, S. Cherubini, V. Crucillà, M. La Cognata, L. Lamia, R.G. Pizzone, S. Romano, M.L. Sergi*

INFN Laboratori Nazionali del Sud, Catania, Italy

DMFCI, Università degli Studi di Catania, Catania, Italy

A. Tumino

INFN Laboratori Nazionali del Sud, Catania, Italy

Università degli Studi di Enna "KORE", Enna, Italy

Li Chengbo

China Institute of Atomic Energy, Beijing, China

Z. Elekes, E. Somorjai

ATOMKI Institute of Nuclear Research, Debrecen, Hungary

V. Burjan, V. Kroha

Nuclear Physics Institute, Academy of Sciences of the Czech Republic, Rez, Czech Republic

A. Mukhamedzhanov

Cyclotron Institute, Texas A&M University, College Station TX, USA

(Dated: September 17, 2010)

Abstract

The quasi-free break-up of deuteron was used to study the neutron induced $^6Li + n$ reaction via the $^2H(^6Li, \alpha^3H)p$. The aim of the experiment was to check whether the deuteron can be considered as a source of virtual neutrons. This was done by studying the excitation function of the $^6Li(n, \alpha)^3H$ two body reaction at low energy where the resonance corresponding to the excited level at $7.454\,MeV$ of ^7Li is present. Two experimental runs were performed at the Laboratori Nazionali del Sud (LNS) in Catania, Italy. In both experiments, the energy and the position of the outgoing α and ^3H particles were measured and the kinematics were reconstructed assuming a proton as third particle. The quasi-free events were selected in order to reconstruct the $^6Li(n, \alpha)^3H$ cross section in the center of mass energy by using the Plane Wave Impulse Approximation approach. The obtained cross section is in very good agreement with the directly measured one.

*Electronic address: spitaleri@lns.infn.it

I. INTRODUCTION

The study of neutron induced reactions is important not only to get information about fundamental nuclear physics but also in applied nuclear physics and nuclear astrophysics. Indeed, neutrons are ideal to probe nuclear interactions avoiding the interference of electromagnetic forces. Moreover, neutron cross sections are relevant for the development of nuclear technologies used for energy production and nuclear waste transmutation. Neutron cross-sections at low energies are also interesting for nuclear astrophysics. For example, all elements heavier than iron were made in environments where neutrons play an important role and the abundance of several light nuclides is modified by (n, γ), (n, p) and (n, α) reactions during the *s*-processes or *r*-processes, or during explosive nucleosynthesis [1, 2].

However, experiments involving neutrons present many problems. Up to now, two complementary methods are mainly used to provide neutron beams. The first method is based on time of flight techniques in connection with neutron sources producing a wide neutron energy range, from nearly thermal energies up to energies in the MeV range. The second method uses charged particle induced nuclear reactions. For example the $^7Li(p,n)^7Be$ reaction can be used to produce neutron energy spectra which simulates a stellar ($kT \approx 25\,keV$) Maxwell-Boltzmann distribution. The on-line detection of the reaction products is often limited by high neutron fluxes. Therefore, the activation technique is frequently used, measuring the characteristic decay of the reaction product, when it is radioactive [3]. Otherwise, new on-line detection techniques have to be used to measure γ-radiation at high neutron fluxes (arrays of BaF_2 detectors not very sensitive to neutron radiation or heavily shielded NaI detectors).
Alternatively, cross sections for some (n, p) and (n, α) reactions can be obtained by studying the reverse reaction and then computing the cross section for the forward one [4]. In this case, a very complex experimental set-up must be used to detect neutrons with good efficiency and resolution.

In this work, the possibility to use the ^2H Quasi-Free (QF) break-up as a source of virtual neutrons is investigated.

QF reactions of light nuclei have been extensively studied in the past at low and intermediate energies in order to investigate the nuclear structure [5–9]. In particular, due to the low binding energy of $n - p$ in deuteron, $n - d$ and $d - d$ break-up reactions have been

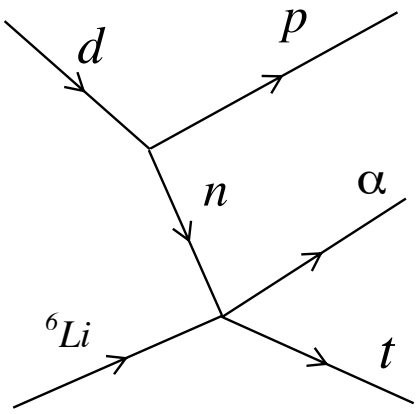

FIG. 1: Pole diagram of the three body reaction studied in the present work.

studied, in order to get information on the $n-n$ and $n-p$ interactions [10–13]. In the last decades, the deuteron QF break-up has been exploited in the framework of the Trojan Horse Method (THM) to study several proton induced reactions at energies relevant for astrophysics, avoiding the Coulomb suppression and the electron screening effects [14–24].

A three-body reaction like:

$$A + a \rightarrow C + c + s, \tag{1}$$

where the nucleus a has a strong $x \bigoplus s$ cluster structure, can proceed through a transfer reaction to the continuum, where the nucleus a breaks up into x and s: x is transferred into the nuclear field of the nucleus A, while s acts as a spectator. This direct process occurs in a restricted region of the three-body phase space, where the momentum of the nucleus spectator s does not change during the reaction, i.e. when the QF reaction conditions are fulfiled. Under these conditions the reaction (1) can be used to determine the cross section of the binary subprocess:

$$A + x \rightarrow C + c. \tag{2}$$

where the nucleus x is a virtual particle.

In the present application the nucleus a is a deuteron, the neutron is the transferred virtual particle ($x = n$), and the proton is the spectator ($s = p$).

Many theoretical approaches, based on the Impulse Approximation (IA) [10, 25], describe this kind of processes using a Feynman diagram. The diagram of the reaction studied in the

present work is shown in fig. 1. The amplitude of the diagram is calculated multiplying two factors: the amplitude of the upper vertex of the diagram, representing the break-up of d into n and p in our case, and that of the lower vertex which describes the virtual two body reaction. The IA is valid if the following conditions are fulfilled: (a) the momentum in the initial channel is sufficiently high or, equivalently, the associated wavelength is smaller than the nuclear radius of the nucleus a, so that the nucleus A can interact only with the cluster x, leaving the other cluster s as a spectator; (b) the incident center of mass energy is higher than the binding energy of the clusters x and s in a.

In Plane Wave Impulse Approximation (PWIA) the three body cross section assumes a simple expression [26–28]:

$$\frac{d^3\sigma}{dE_c d\Omega_c d\Omega_C} \propto KF|\phi_a(p_{sx})|^2 \left(\frac{d\sigma}{d\Omega_{c.m.}}\right)^{HOES} . \tag{3}$$

In eq. (3) KF is a kinematical factor, depending on masses, momenta and angles of the outgoing particles, that takes into account the final state phase-space factor:

$$KF = \frac{\mu_{Aa} m_c}{(2\pi)^5 \hbar^7} \frac{p_C p_c^3}{p_{Aa}} \Big[\Big(\frac{\overrightarrow{p}_{Bx}}{\mu_{Bx}} - \frac{\overrightarrow{p}_{Cc}}{m_c} \Big) \cdot \frac{\overrightarrow{p}_c}{p_c} \Big]^{-1} \tag{4}$$

where p_j, m_j are the momentum and the mass of particle j; $\overrightarrow{p}_{ij}$ and μ_{ij} are the relative momentum and the reduced mass of particles i and j and B denotes the $C + c$ system (see (1)). $\phi_a(p_{sx})$ is the Fourier transform of the radial wave function for the $x - s$ inter-cluster motion inside a, usually described in terms of the Hulthén function for deuteron [23]. The $(d\sigma/d\Omega_{c.m.})^{HOES}$ factor is the differential cross section for the two body reaction (2) at the relative energy E_{xA} of the two particles in the entry channel (x and A) and at the center-of-mass reaction angle θ_{cm} of the two-body reaction. The two-body cross section is half-off-energy-shell (HOES), because of the off-shell character of x in the entry channel.

The angle θ_{cm} is calculated as [31]:

$$\theta_{c.m.} = \arccos \frac{(\vec{v}_A - \vec{v}_x) \cdot (\vec{v}_C - \vec{v}_c)}{|\vec{v}_A - \vec{v}_x||\vec{v}_C - \vec{v}_c|} \tag{5}$$

where the vectors $\vec{v}_A$, $\vec{v}_x$, $\vec{v}_C$, $\vec{v}_c$, are respectively the velocities of projectile, transferred cluster and outgoing particles.

The relative energy E_{xA} is given by [15, 16, 20]:

$$E_{xA} = E_{cC} - Q_{2b} \tag{6}$$

where Q_{2b} is the Q value for the binary reaction (2) and E_{cC} is the relative energy of the outgoing particles c and C. The relative momentum of the on-shell exit particles (c and C) is related to their relative energy by $k_{Cc} = \sqrt{2\mu_{Cc}E_{Cc}}$. Indeed, the relative momentum of the entry particles (A and x), due to the off-shell character of x, is compensated for by the binding energy of x and s inside a (ϵ_{xs}) and it results $E_{xA} = \frac{k_{xA}^2}{2\mu_{xA}} - \epsilon_{xs}$.

The distorted wave impulse approximation (DWIA) treatment [28, 29] was sometime applied to describe QF reactions. In the DWIA the radial wave functions are deduced from optical-model potentials, so that the $|\phi_a(p_{sx})|^2$ in eq. (3) becomes dependent on the considered reaction as well as on the energy. However, it should be stressed that the main differences between the momentum distributions calculated in PWIA and DWIA are in the tails and in the absolute value [16, 30]. Furthermore, the eq. (3) prevents the extraction of the absolute value of the two body cross-section. However, the absolute magnitude of the cross-section can be derived from a scaling to the direct data, in an energy range where they are available. Thanks to this, as only the region of low momentum p_s for the spectator is selected in the data analysis ($|p_s| < 20 MeV/c$ in this work), where the $|\phi_a(p_{sx})|^2$ distributions are coincident, the more simple PWIA approach was used in the present study.

In order to study the cross section of neutron induced reactions we have to select the QF reaction channel in the three body reaction. In this way, it is possible to get a measurement of a neutron induced reaction cross section using deuterons as a virtual source of neutrons and avoiding the experimental problems coming from the use of neutron beams and/or neutron detectors. Preliminary studies of the $^2H(^6Li, \alpha^3H)p$, $^2H(^{17}O, \alpha^{14}C)p$ reactions have been performed, checking the possibility to retrieve information on the cross section of the ^6Li+n and $^{17}O + n$ two-body reactions [32–35].

In this paper, a detailed study of the $^6Li(n, \alpha)^3H$ reaction via the $^2H(^6Li, \alpha^3H)p$ three body reaction is presented. The experimental conditions were chosen to satisfy the validity conditions of the IA. Indeed, the energy of the ^6Li beam of $17 MeV/c$ corresponds to a $^6Li - d$ relative wavelength of $1.8 fm$, much smaller than the deuteron effective radius of $4.5 fm$. The studied reaction represents a good benchmark to verify this new application of the QF reaction mechanism, since the directly measured data show a resonance in the cross section at about $E_{^6Li-n} = 210\ keV$ with a FWHM of 100 keV, corresponding to the excited level at 7.454 MeV of ^7Li. The aim of this study is to reproduce the resonance cross section with a resolution comparable with the directly measured one.

TABLE I: Details of the set-up used for the two different measurement runs.

	first run	second run
Beam Energy	14 MeV	17 MeV
Target Thickness	$150\,\mu g/cm^2$	$100\,\mu g/cm^2$
ΔE Si Detectors Thickness	$20\,\mu m$	—
E Si PSD detectors Thickn.	$1000\,\mu m$	$1000\,\mu m$
Detection Angular Ranges	$18° - 28°$	$22° - 25°$
	$43° - 53°$	$36° - 39°$
Angular resolution	$\pm 0.1°$	$\pm 0.05°$
Rel. energy ($E_{^6Li-n}$) range	0 - 1.5 MeV	0 - 0.3 MeV
Experimental $E_{^6Li-n}$ uncertainty (resolution of the method)	$\pm 60\,keV$	$\pm 15\,keV$

II. THE EXPERIMENT

Two measurements of the $^6Li + d \rightarrow \alpha + t + p$ reaction were performed at Laboratori Nazionali del Sud (LNS) in Catania. In both experimental runs, a ^6Li beam was delivered by the SMP Tandem Van de Graaf on a CD_2 target. The angular positions and the energies of the two ejectiles, α and ^3H, were detected in coicidence using two Position Sensitive silicon Detectors (PSDs, single area, resistive readout) having a spatial resolution of 0.5 mm. The two detectors were placed on opposite sides with respect to the beam axis direction.

The details of the experimental set-up used in the two experimental runs, together with the relative energy $E_{^6Li-n}$ range exploited by the experimental apparatus are reported in tab. I.

In the first experiment [32] the two ejectiles, α and ^3H, were identified using two $\Delta E - E$ Si telescopes. Events produced by the QF break-up of a deuteron were selected and the two body cross section for the $^6Li + n \rightarrow t + \alpha$ reaction was reconstructed. Since the energy uncertainty achieved by the indirect measurement was higher than that presented by the direct one, the direct data [36] were smeared out at the same uncertainty of the indirect ones, in order to make a comparison of the two data sets. The result reported in ref. [32] shows a good agreement.

The second experiment was devoted to the measurement of the resonance. The aim was to reproduce the resonance width with a resolution comparable with the directly measured one. To found the best experimental conditions, a detailed kinematical simulation of the $^2H(^6Li, \alpha^3H)p$ reaction was performed taking into account the experimental uncertainties coming from the finite dimension of the beam spot, the energy and angular spread of both beam and ejectiles in the target and the angular and energy resolution of the detectors. The beam energy and the experimental set-up were then chosen such that the *"magnifying glass"* effect [37] can be exploited to achieve a resolution better than that of the first experiment in the ^6Li-n relative energy variable, $E_{^6Li-n}$. Indeed, under proper kinematical conditions, it is possible to translate a slow variation in relative energy of the two outgoing particles ($E_{t\alpha}$ in our case) into a large variation of energy of the ejectiles (E_t and/or E_α). This effect allows to accurately study the variation of the cross section as a function of $E_{^6Li-n}$. As the simulations have shown the strong dependence of the $E_{^6Li-n}$ measurement uncertainty on the angular resolution of both ejectiles, the experimental set-up was designed to reduce the uncertainties in the measurement of angles. The beam spot was reduced to $1\,mm$ in diameter using a collimator and an anti-scattering system. Thanks to the diameter of the scattering chamber ($2000\,mm$), the two PSDs were placed at a distance of $780\,mm$ from the target. A holder designed for this purpose was used to fix both PSDs together with two point-like silicon detectors, placed at 8° on both side with respect to the beam direction. The measurement of the $^6Li + d$ elastic scattering in the point-like detectors gave the possibility to check the position of the detectors holder and to monitor the beam direction and the target during the experiment. Moreover, the beam energy and the detectors angular ranges were chosen such that ^3H and α particles can be identified by kinematics, avoiding the use of ΔE detectors and hence the straggling effects affecting the detected particles.

In the second experiment, thanks to the described set-up and the chosen kinematical conditions, the overall resolution was enhanced. An angular resolution of the outgoing particles of about 0.1° (FWHM) was achieved. Moreover, taking into account all the experimental uncertainties, the energy $E_{^6Li-n}$ was measured with an uncertainty of $30\,keV$ (FWHM), though the investigated range was reduced with respect to the first experiment.

The energy and position signals of the PSDs were processed by standard electronics together with the delay between the time signals coming from the two PSDs. The trigger for the data acquisition was given by the coincidence between the two PSDs. The signals

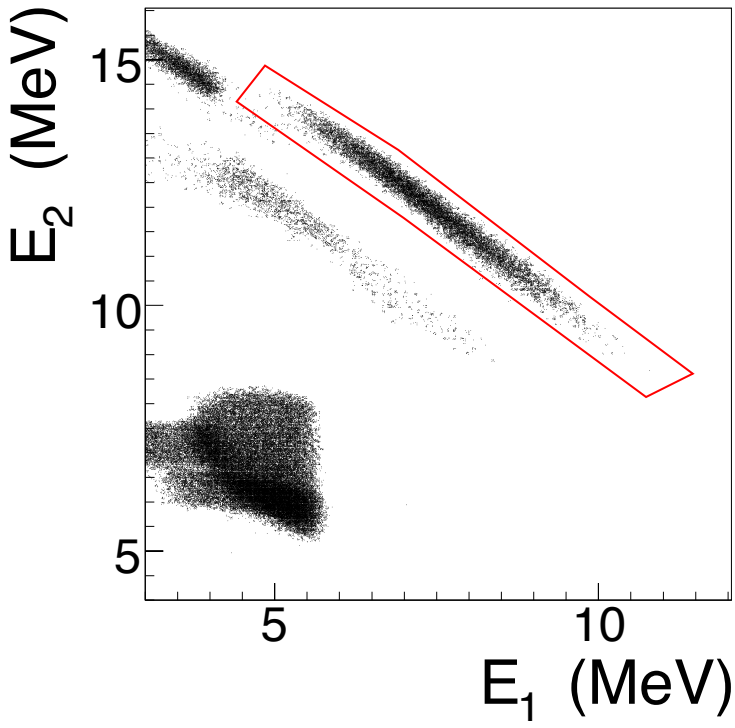

FIG. 2: Correlation spectra of the energies detected by the two PSD detectors. The selection of the kinematical locus of interest is superimposed on the data (full line).

were then sent to the acquisition system for on-line monitoring and data storing.

In the following, only data from the second experimental run will be presented.

III. DATA ANALYSIS

A. Detector calibration and identification of the $^2H(^6Li, \alpha^3H)p$ reaction

The PSDs used in the experiment were calibrated in energy using the elastic scattering peaks measured at different beam energies for the $^6Li + ^{197}Au$, $^6Li + ^{12}C$ reactions and the $^6Li + ^{12}C \rightarrow ^{14}N^* + \alpha$ reaction. Moreover, a three peaks alpha source ($^{239}Pu - ^{241}Am - ^{244}Cm$) was used to calibrate at low energies.

The angular calibration was performed using grids with equally spaced slits placed in front of each PSD during the calibration runs. This allows to establish a correspondence between position and angle.

The beam spot and its energy spread on the target were also taken into account for the

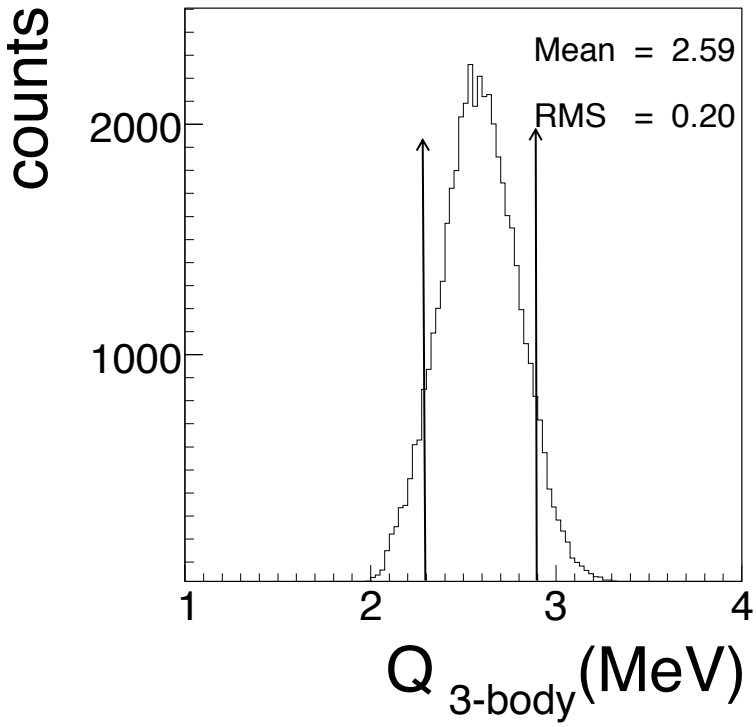

FIG. 3: Q-value plot for the events falling in the kinematical locus corresponding to the ${}^6Li + d \rightarrow \alpha + {}^3H + p$ reaction.

calibration in position and energy, as well as the detected particle energy loss on the target and on the dead layer of the detectors.

After detector calibration, to identify the events corresponding to the 3-body reaction of interest ${}^6Li + d \rightarrow \alpha + {}^3H + p$, the correlation spectrum of the energies measured by the two PSDs was checked (see Fig. 2). The kinematical locus that corresponds to the channel of interest is clearly separated from the background and from the kinematical locus corresponding to the ${}^6Li + d \rightarrow \alpha + {}^3He + n$ reaction. For the events falling into the region defined by the solid line in fig. 2, the Q-value was reconstructed under the hypothesis of a proton as third particle, and it is shown in fig. 3. It is centered at $2.59 \pm 0.20\,MeV$, to be compared with the theoretical value of $2.558\,MeV$. The good agreement between the experimental and the theoretical Q-values confirms the identification of the reaction channel and the accuracy of the detector calibration. The identification of the events belonging to the reaction under study is done by using a selection cut on the Q-value. In the following, only events falling between the two solid lines shown in fig. 3 are considered. Moreover,

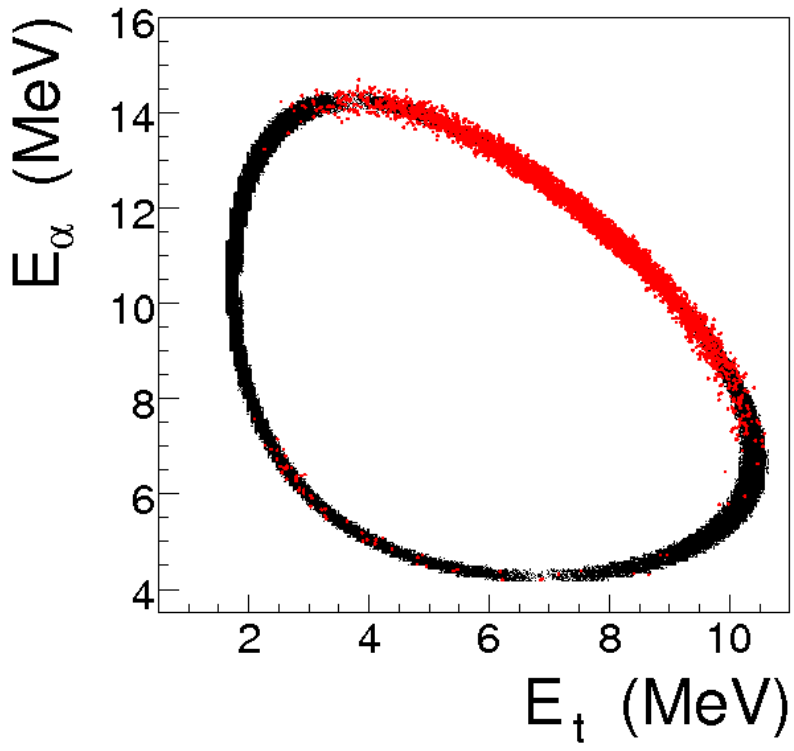

FIG. 4: Comparison between the experimental data (red points) that satisfy the Q-value and the TAC cuts (see text) and the kinematical calculation for the ${}^6Li + d \rightarrow \alpha + {}^3H + p$ reaction.

to further select the events of interest, a cut on the time delay between the signals coming from the two PSDs was used (TAC).

To check the identification conditions, a comparison between the selected experimental data and the kinematical calculation for the ${}^6Li + d \rightarrow \alpha + {}^3H + p$ reaction was performed for several angular pairs of the two outgoing particles. A typical spectrum of energy correlation is shown in fig. 4, where the black region represents the result of the kinematical calculation, and the red points are the experimental data. The agreement between the two data sets confirms the good identification of the reaction of interest.

B. Experimental evidence of the QF-mechanism

The ${}^6Li + d \rightarrow \alpha + {}^3H + p$ reaction can in principle proceed through the processes shown in fig. 5. In the figure the deuteron break-up is represented in (a), and the sequential processes (SP) through the excited states of ${}^7Li$ and ${}^4He$ and the ground state of ${}^5Li$ are sketched

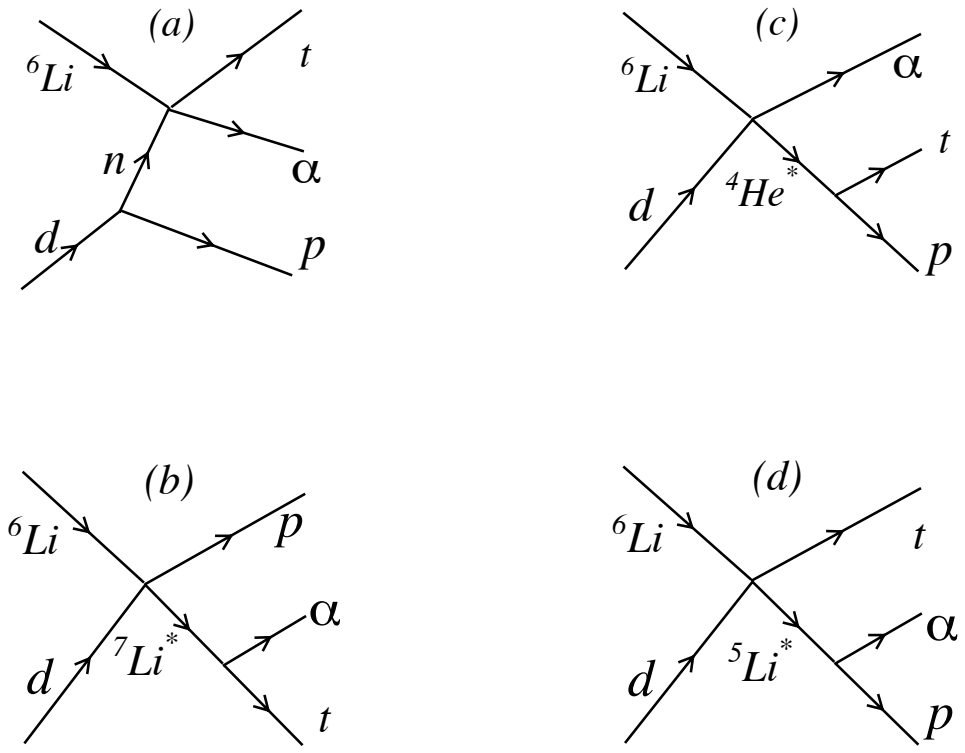

FIG. 5: Simplified schema of the QF $^2H(^6Li, \alpha^3H)p$ reaction (a) and of other possible competitive channels feeding the same particles in the final states: $^6Li(d,p)^7Li^*$,$^7\,Li^* \rightarrow \alpha +^3 H$ (b), $^6Li(d,\alpha)^4He^*$,$^4\,He^* \rightarrow p +^3 H$ (c), $^6Li(d,^3\,H)^5Li$,$^5\,Li \rightarrow \alpha + p$ (d).

in $(b), (c), (d)$, respectively. After selecting the events corresponding to the $^2H(^6Li, \alpha^3H)p$ reaction, it is then necessary to verify if the QF reaction process is present and if it can be discriminated from other ones feeding the same particles in the final state.

For this purpose, several tests were carried out to assess if the necessary conditions for the presence of QF processes were fulfilled and to identify the events corresponding to the QF process. These tests are reported in the following sections.

1. Relative energy two-dimensional plots

In order to investigate the possible presence of SP, the correlations between the relative energy of two out of three outgoing particles calculated in post collision prescription are checked for fixed values of the angles of the outgoing particles θ_α and $\theta_{^3H}$. For all the angular pairs a clear vertical locus, corresponding to the excited level of ^7Li under study,

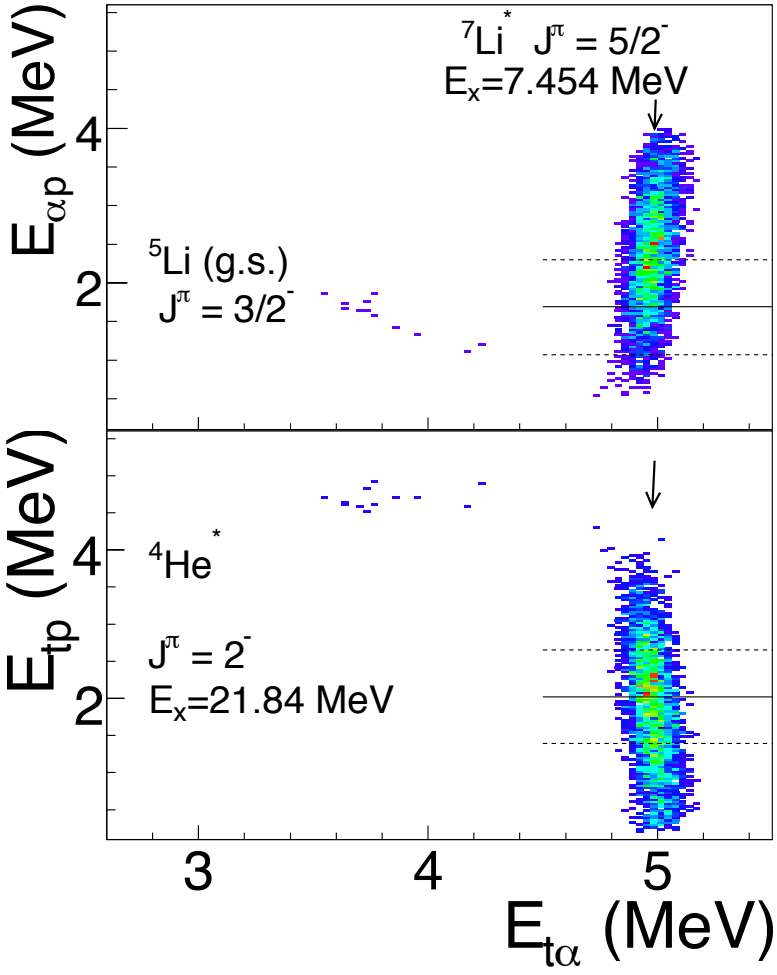

FIG. 6: Correlation plots for the relative energies $E_{^3Hp}$ vs $E_{^3H\alpha}$ and $E_{\alpha p}$ vs $E_{^3H\alpha}$ for $\theta_{^3H} = 38.5° \pm 0.5°$ and $\theta_\alpha = 23.3° \pm 0.5°$. The solids lines represent the position of the third excited state of ^4He and the g.s. of ^5Li. No signal of other ^4He or ^5Li states can be found in the data. The arrows indicate the position of the ^7Li excited state under investigation.

is present. Small contributions due to the 2^- state of ^4He and to the g.s. of ^5Li were also found.

The typical two dimensional plots, E_{tp} vs $E_{t\alpha}$ and $E_{\alpha p}$ vs $E_{t\alpha}$, for $\theta_{^3H} = 38.5° \pm 0.5°$ and $\theta_\alpha = 23.3° \pm 0.5°$ are reported in Fig. 6. For this angular pair, the momentum of the spectator in the 3-body reaction has its minimum at $0 MeV/c$. The condition of zero proton momentum is requested for QF reaction because the deuteron has a predominant component in s wave, so the momentum distribution of $p-n$ system in the deuteron has a maximum for

$p_s = 0\ MeV/c$. The angular pairs $(\theta_\alpha, \theta_{^3H})$ which fulfill this condition are called quasifree angles.

In Fig. 6 the locus due to the excited level of ^7Li is indicated by a vertical arrow. The horizontal solid lines show the relative energy corresponding to the ground state of ^5Li (upper panel) and the 2^- state of ^4He at excitation energies $21.84MeV$ (lower panel), and the dashed lines represent the FWHM of the reported states. Small contributions due to the 2^- state of ^4He are visible in the figure. Similar plots are obtained for any other angular pair of the ejectiles and no other contributions from ^4He or ^5Li states were found in the data.

2. Study of the coincidence yield

A quantitative analysis of the presence of SP and QF mechanism was performed studying the coincidence yield of the three body reaction projected on different variables for fixed values of θ_α and θ_t. The spectra were fitted by incoherently adding, with free weights, the contributions of SP and QF reactions (see fig. 5) calculated using a Monte Carlo simulation. In particular, the coincidence yields for SP were described assuming a Breit-Wigner shape for the spreading of the ^4He, ^5Li and ^7Li levels involved in the 3-body reaction, and to describe the QF process the eq. (3) was used. For each fixed pair (θ_α, $\theta_{^3H}$) the fit was firstly performed for the E_α spectrum, and the obtained weights for the different SP and QF processes were used to reproduce the $E_{^3H}$, E_{tp} and $E_{\alpha p}$ spectra.

As an example, in fig. 7(a) the fit of the coincidence yield as a function of E_α for the QF angular pair $\theta_{^3H} = 38.5^\circ \pm 0.5^\circ$ and $\theta_\alpha = 23.3^\circ \pm 0.5^\circ$ is shown. The full line represents the results of the fit, the dashed line shows the QF reaction contribution, and the dotted and the dashed-dotted lines show the contributions of SP due to the population of the 2^- state of ^4He and the g.s. of ^5Li, respectively. In fig. 7 (b),(c),(d), the coincidence yield as a function of $E_{^3H}$, E_{tp} and $E_{\alpha p}$ is compared with the incoherent sum (full lines) of the Monte Carlo calculations for SP and QF processes weighted using the parameters obtained from the fit of fig. 7 (a). No adjustment of these parameters was done to obtain the solid lines in fig. 7 (b),(c) and (d).

The agreement between data and simulation gives us confidence of the goodness of the fit results. As before, the contribution of QF mechanism is represented by a dashed line, while

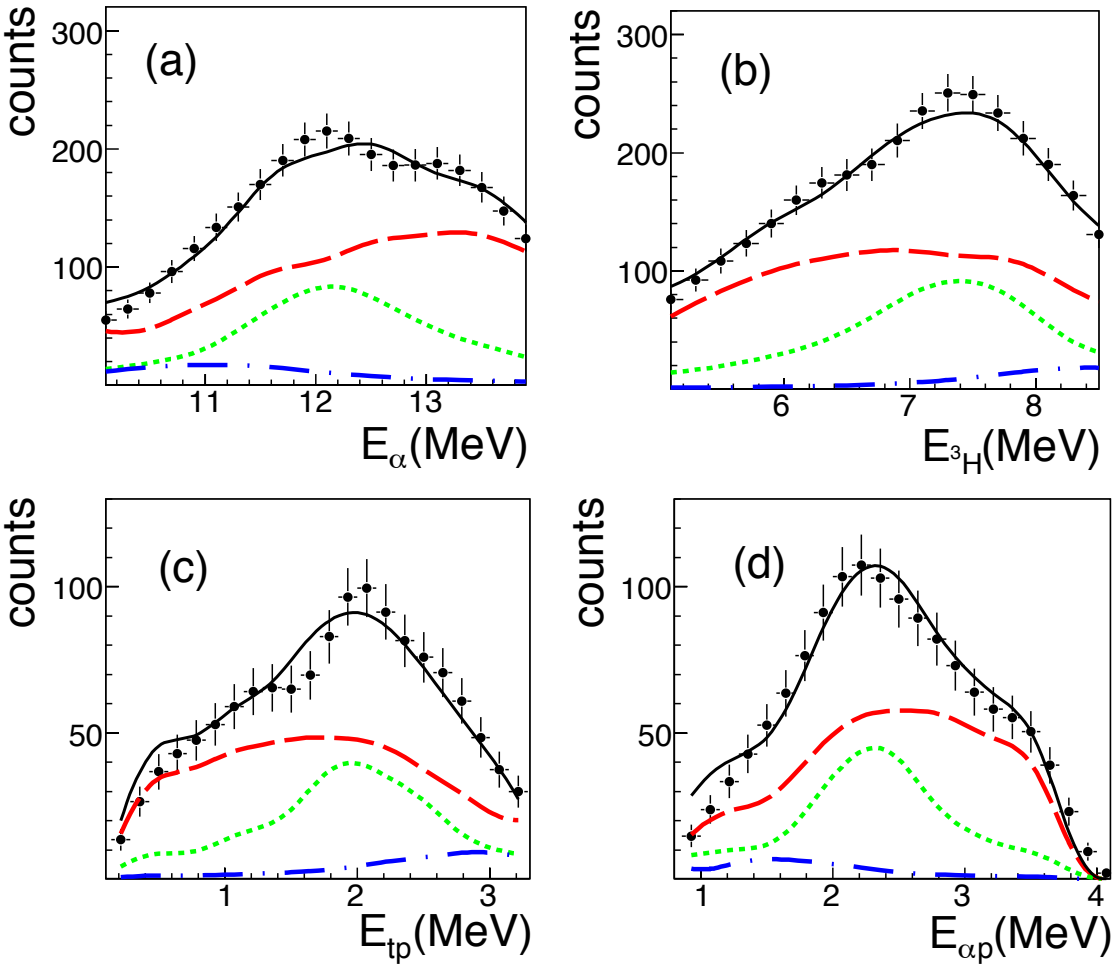

FIG. 7: Typical coincidence spectra projected on E_α, $E_{^3H}$,$E_{\alpha n}$ and E_{tn} for $\theta_\alpha = 23.3° \pm 0.5°$ and $\theta_{^3H} = 38.5° \pm 0.5°$. In panel (a), the full line is a fit of the coincidence yield in the E_α variable obtained by taking into account SP (dotted and dash-dotted lines) as well as QF (dashed line) contributions summed incoherently. In panel b, c, d the data are represented as a function of the other variables. A remarkable agreement between the data and the incoherent sum (solid lines) obtained using the same parameters as in a of SP (dotted and dash-dotted lines) and QF contribution (dashed line) is clearly shown for all the variables.

the dotted and dash-dotted lines represent the SP contributions coming from population of α^* and ^5Li, respectively. Similar results are obtained for the other angular pairs.

The fit of the coincidence yields returns in average a 69% contribution of QF reaction for the QF angular pairs. For angular pairs out of the QF ones, this contribution decreases in average down to 33%.

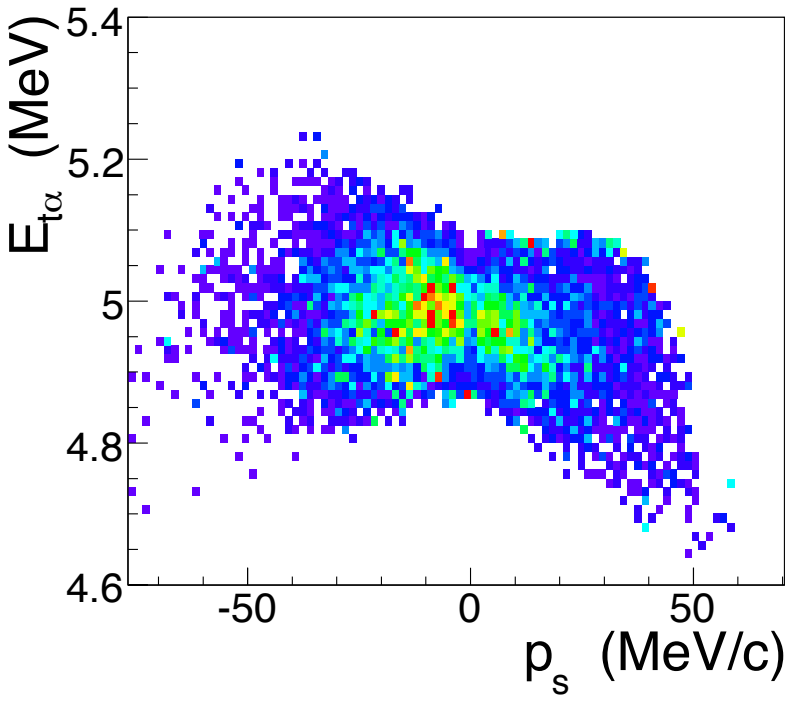

FIG. 8: The scatter plot of the three-body reaction yield weighted by the phase space contribution as a function of $E_{t\alpha}$ and p_s.

This result confirms the predominance of the QF process over the SP for the QF-angles, so in the following only events falling into the QF angular pairs will be considered. Moreover, the contributions due to the SP are subtracted in the following analysis.

3. Data as a function of momentum of the spectator

A complementary way to test the presence of the QF mechanism and/or SP is to investigate the correlation between the relative energy $E_{t\alpha}$ and the momentum of the proton p_s (see fig. 8). The figure shows that the main contribution to the $7.454\,MeV$ state of ^7Li is obtained for very low values of p_s, when the proton acts as spectator, as it is expected for QF reaction mechanism. The scatter plot in fig. 8 shows the three-body reaction yield weighted by the phase space contribution (see eq. 3) as a function of $E_{t\alpha}$ and p_s.

The correlation plot was than projected onto the $E_{(t\alpha)}$ relative energy for different ranges of p_s, and the results are shown in fig. 9. The three-body coincidence yield divided by the phase space factor appears to be higher for $|p_s| < 20MeV/c$ rather than for $20 < |p_s| <$

$40 MeV/c$ and $40 < |p_s| < 60 MeV/c$. This behaviour represents a necessary condition for the predominance of the QF mechanism with respect to SP.

When the QF reaction mechanism is predominant and a PWIA approach can be used, the three body cross section is described by eq. 3. Consequently, the three-body reaction yield divided by the phase space contribution is proportional to the product of the differential two-body cross section and the p_s momentum distribution:

$$\frac{d^3\sigma}{dE_c d\Omega_c d\Omega_C} \frac{1}{KF} \propto |\phi_a(p_{sx})|^2 \left(\frac{d\sigma}{d\Omega_{c.m.}}\right)^{HOES} . \tag{7}$$

The integral of this quantity with respect to $E_{t\alpha}$ ($< |\phi_a(p_{sx})| >^2$) should then be modulated by the momentum distribution of $n - p$ on d, described in s-wave by the Fourier transform of the Hulthén function:

$$\phi(p_s) = \frac{1}{\pi} \sqrt{\frac{ab(a+b)}{(a-b)^2}} \left[\frac{1}{a^2 + p_s^2} - \frac{1}{b^2 + p_s^2}\right] \tag{8}$$

The integrals of the histograms in fig. 9 are reported in fig. 10 as a function of the spectator momentum p_s and compared with the expected Hulthén function. The full line represents the Hulthén function with the asymptotic parameters ($a = 0.2317 fm^{-1}$, $b = 1.202 fm^{-1}$) [23], while the dashed line reports the Hulthén function with a width of 54 MeV/c expected if the final state interaction for low transferred momenta is taken into account [38–40]. A good agreement is evident and gives once more confidence that, in the investigated kinematical region, the QF mechanism gives the main contribution and that it can be disentangled from the SP contributions.

4. Analysis of the proton momentum distribution

A final and more sensitive check of the predominance of the QF reaction mechanism is achieved by investigating the shape of the experimental momentum distribution of the proton inside deuteron. Indeed, this observable is very sensitive to the reaction mechanism. The experimental momentum distribution can be obtained by dividing the three body coincidence yield by the phase space factor in a kinematical region where the two body cross section can be approximated to a constant (see eq. 7). This is done by considering steps of 30 keV in the $E_{t\alpha}$ variable and steps of 10° in θ_{cm}. The experimental distribution is shown in fig. 11 as full dots, and compared with the Hulthén function normalized to the data. As before,

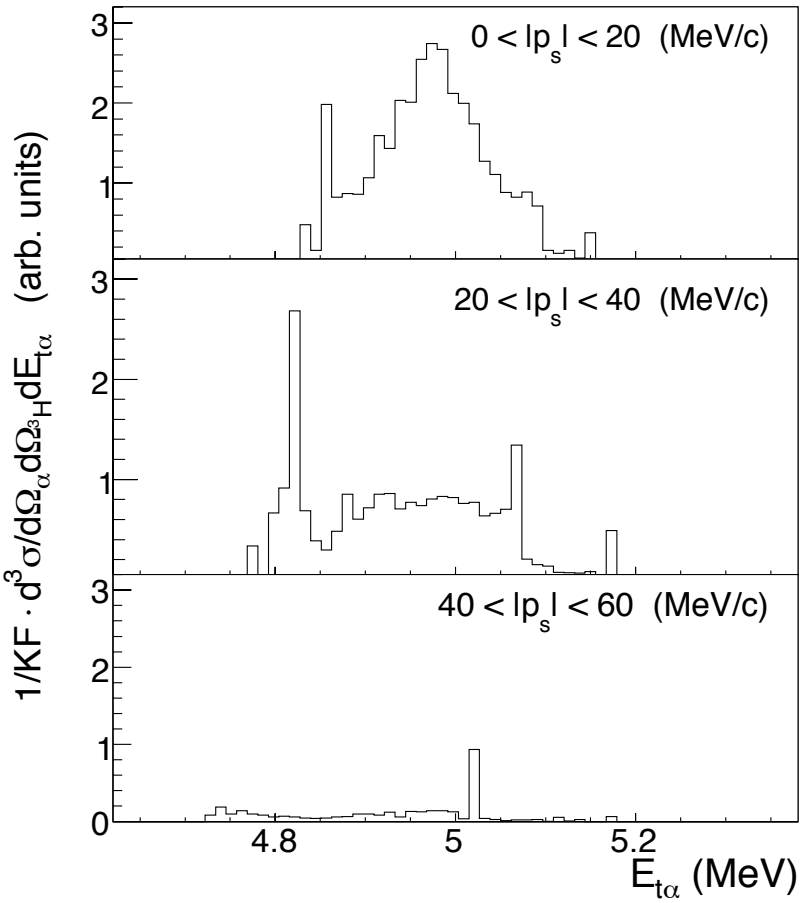

FIG. 9: Coincidence yield divided by the phase space factor projected on $E_{t\alpha}$ for $0 < |p_s| < 20\,MeV/c$ (upper panel), $20 < |p_s| < 40\,MeV/c$ (central panel), $40 < |p_s| < 60\,MeV/c$ (bottom panel).

the full line represents the Hulthén function for the asymptotic parameters [23], while the dashed line reports the Hulthén function with the width expected at the used beam energy [38–40]. The agreement between the experimental data and the predicted distribution is good. This last test gives further evidence on the validity of the procedure used for the selection of the data where the QF contribution is dominant. We note that the momentum distribution of the spectator in the deuteron generated by the Hulthén potential coincides with the one obtained using realistic Reid soft-core potential at $|p_s| < 40 MeV/c$

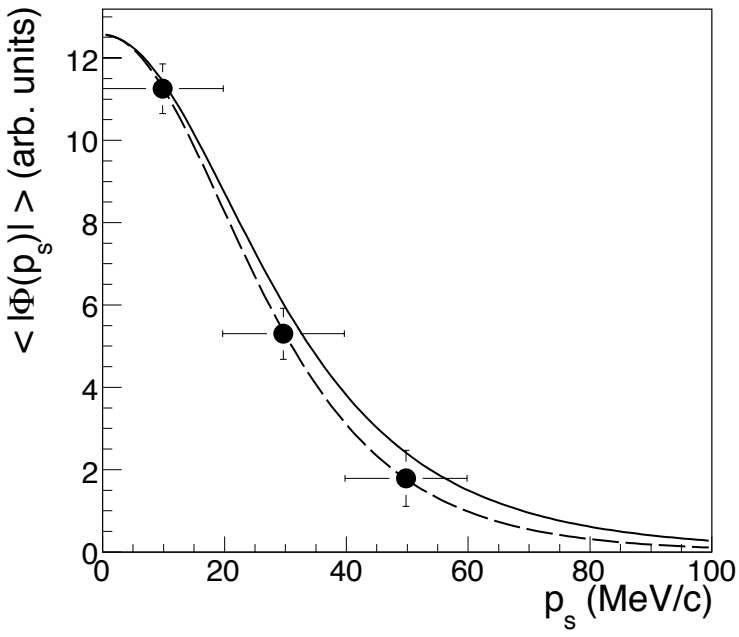

FIG. 10: Integral with respect to $E_{t\alpha}$ of the coincidence yield divided by the phase space factor as a function of the momentum of the spectator. The solid line represents the theoretical Hulthén function and the dashed line represents the Hulthén function with a width of $54\,MeV/c$ [38].

IV. EXPERIMENTAL RESULTS

The experimental tests described in the previous section demonstrated that: (i) the QF mechanism is present in a subset of the experimental data; (ii) the QF mechanism represents the main contribution to the $^6Li + d \rightarrow t + \alpha + p$ reaction if the kinematical region around the QF angular pairs is selected; (iii) the QF contributions can be disentangled from the contaminant component due to SP. Further data analysis was then performed only for these data.

Moreover, only coincidence events with $|p_s| < 20 MeV/c$, corresponding to a center-of-mass angular range $\theta_{cm} = 95^\circ - 110^\circ$, were considered. As a consequence a simple analysis in PWIA can be used to describe the selected subset of experimental data.

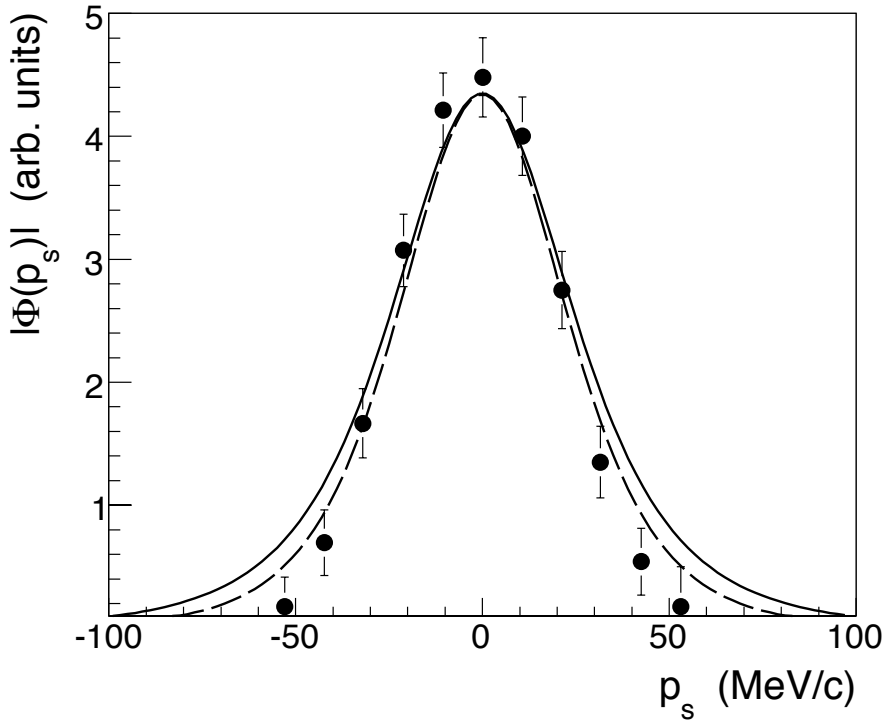

FIG. 11: Reconstructed momentum distribution of the undetected proton inside the cluster nucleus deuteron. The solid line represents the theoretical Hulthén function and the dashed line represents the Hulthén function with a width of $54\,MeV/c$ [38].

A. Extraction of the two-body indirect cross section.

The last step of the data analisys is the extraction of the HOES cross section of the $^6Li+n \rightarrow ^3 H+\alpha$ binary reaction. From eq. (3), the two-body cross section in arbitrary units can be derived by dividing the selected three body coincidence by the factor $KF|\phi_a(p_s)|^2$. This factor is calculated using a Monte Carlo simulation. The geometrical efficiency of the experimental set-up together with the thresholds of the detectors were taken into account in the simulation. The momentum distribution used in the calculation corresponds to the dashed line in fig. 10 and fig. 11. We stress once again that only events with $|p_s| < 20\,MeV/c$ are accepted in the data analysis.

The on-energy-shell (OES) $^6Li + n$ reaction is contributed by resonant and nonresonant (direct) mechanisms. At low energies the $J^\pi = 5/2^-$ resonance in ^7Li at $E_{^6Li-n} = 204keV$ dominates. The resonant reaction is characterized by the orbital angular momentum in the initial (final) state $l_i = 1$ ($l_f = 3$). At very low energies due to the threshold behavior of

the neutron induced direct reaction cross section $\sigma \propto k_i^{2l_i-1}$, where k_i is the ^6Li-n relative moment, the $1/k_i$ tail from the direct mechanism with $l_i = 0$ will prevail. To compare the result obtained in the present work with the OES cross section, the indirectly measured two-body cross-section was corrected for the neutron penetrability factor of the centrifugal barrier, which is missing in the THM two-body cross section. The centrifugal barrier is given by:

$$P_{l_i} = \frac{1}{k_i r(j_{l_i}(k_i r)^2 + n_{l_i}(k_i r)^2)} \tag{9}$$

calculated for $l_i = 1$, where $j_{l_i}(k_i r)$ and $n_{l_i}(k_i r)$ are respectively the spherical Bessel and Neumann functions and r is the channel radius. In the calculations the value $r_{^6Li} = 2.09 fm$ from ref. [41] was used as interaction nuclear radius of ^6Li.

Moreover, as in the THM measurement the neutrons take part to the reaction as off-shell particles, a function representing the $1/v$ dependence of the cross section for slow neutrons was introduced in the indirect data. In fig. 12, the indirect two-body cross section is compared with the experimental direct data. As the center of mass angular region covered by the indirect measurement is not very large, the comparison was performed with the direct data integrated over the same range of θ_{cm} ($\theta_{cm} = 95° - 110°$) [36]. The indirect two body cross section and the directly measured one present the same energy uncertainty, so the comparison of the two data sets was performed without smearing out the direct data at a larger energy bin, as it was done to compare the direct data with those coming from the first experimental run [32]. Since eq. (3) does not allow to extract the absolute value of the cross section, the indirect data are normalized to the direct ones. The normalization factor is calculated in the energy region where the resonance is present so that the areas of direct and indirect measured resonance peaks are equal. The two data sets show a very good agreement, and the indirect measurement successfully reproduces both the energy of the resonance peak and its FWHM.

The two body cross section obtained in this work was fitted using a sum of a Breit-Wigner function and a function $\propto 1/\sqrt{E}$ that describes the cross section for slow neutrons induced reactions. The result is shown in fig. 13, where the full line gives the total fit function, while the dotted and dashed line are the Breit-Wigner and the $1/\sqrt{E}$ functions respectively. The fitting procedure returns a resonance centered at energy of $204 \pm 4\, keV$ with a FWHM of $96 \pm 8\, keV$, in excellent agreement with the fit performed on the direct data.

As the correction for the centrifugal barrier depends on the value of the channel radius,

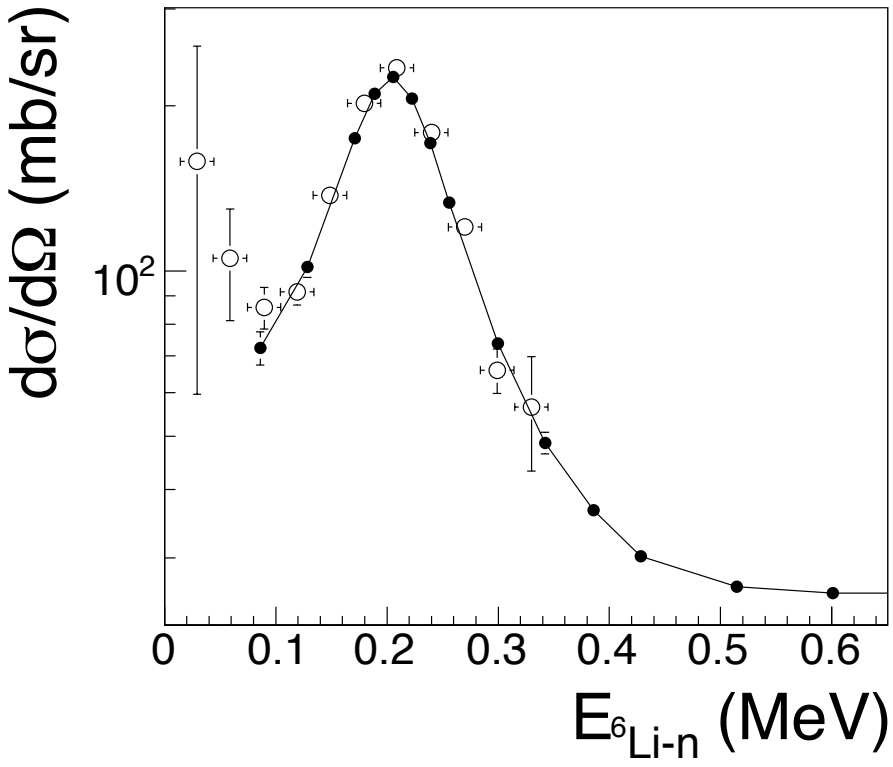

FIG. 12: Two body cross section obtained in this work (open circles) compared with the directly measured one (full dots) integrated over the center of mass angular region $\theta_{cm} = 95° - 110°$. The line just guides the eye.

several calculations were performed on varying this parameter from $2\,fm$ up to $10\,fm$. In the region of the resonance, the change of channel radius gives a small shift of the maximum of the resonance (about $2\,keV$), while the width of the resonance remains unchanged.

V. CONCLUSIONS

A new application of the QF reaction mechanism to study neutron induced reactions is shown in this work. In particular the ^6Li+d reaction was studied at LNS to get information about the ^6Li+n processes by using the break-up of ^2H. Since the ^6Li+n excitation function presents a very well known resonance corresponding to the ^7Li excited level at $7.454\,MeV$, this reaction is a good benchmark for the method. In order to reproduce the central value and the width of the resonance with a resolution comparable with that of the direct data, the experiment was optimized reducing the experimental uncertainties. To achieve a very

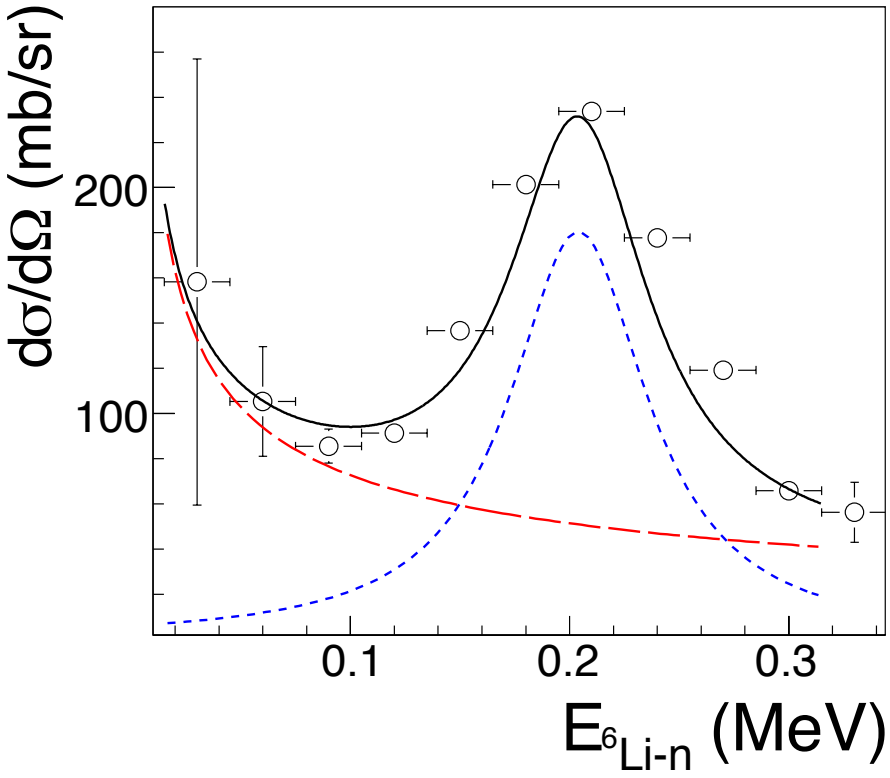

FIG. 13: Two body cross section fitted by a Breit-Wigner peak (dotted line) on a function $\propto 1/\sqrt{E}$ (dashed line). The full line represents the total fit function and the dots are the experimental data.

good resolution in the measurement of the angles of the outgoing particles, the detectors were placed at $800\,mm$ from the target. In addition, the beam energy and the detection angles were fixed so that the identification of the reaction channel of interest was achieved by means of kinematics, avoiding the use of ΔE detectors. Moreover, the *"magnifying glass"* effect was used in order to increase the $E_{^6Li-n}$ energy resolution with respect to the previous experiment [32].

A careful analysis was performed taking into account the beam spot and the beam energy spread on the target, the energy loss of the detected particles in the target and in the dead layers of the detectors.

The agreement between the $^6Li(n,\alpha)^3H$ cross section obtained in this work and the direct one in the same two-body center of mass angular region is very good. This demonstrates that using an indirect method it is possible to reach a good resolution in measuring the cross section of two body reactions induced by neutrons. This result represents an important test

in view of further applications to key neutron induced reactions in nuclear astrophysics using deuterons as a virtual source of neutrons. This technique is particularly interesting when applied to processes involving radioactive species. Indeed, such studies can not be performed with direct methods when the radioactive species have short lifetime (order of minutes or less).

VI. ACKNOWLEDGMENTS

The authors would like to thank the technical staff of the Laboratori Nazionali del Sud for its invaluable assistance. ZE and ES acknowledges support from OTKA (T49245). AM acknowledges the support of the US Department of Energy under Grant No. DE-FG02-93ER40773 and DE-FG52-06NA26207, NSF under Grant No. PHY-0852653. VB and VK acknowledge the support of Grant LC 07050 of the Czech MSMT.

[1] I. Iben, Astrophys. J. **196**, 525 (1975)

[2] F. Kppeler, F-K Thielemann, M. Wiescher, Ann. Rev. Nucl. Part. Sci. **48**, 175 (1998)

[3] H. Beer et al., Nucl. Inst. Meth. **A337**, 492 (1994)

[4] J. H. Gibbons and R.L. Macklin, Physic. Rev. **114**(2), 571 (1959)

[5] G. Jacob, TH.A.J. Maris, Rev. Mod. Phys. **38**(1), 121 (1966)

[6] D. J. Milijanic et al., Nucl. Phys. **A215**, 221 (1973)

[7] J. Kasagi et al., Nucl. Phys. **A239**, 233 (1975)

[8] I. Slaus et al., Nucl. Phys. **A286**, 67 (1977)

[9] M. Lattuada et al., Nucl. Phys. **A458**, 493 (1986)

[10] G.F. Chew et al., Phys. Rev. **80**, 196 (1950)

[11] B. Zeitnitz, R. Maschuw, P. Suhr, W. Ebenhoh, Phys. Rev. Lett. **28**, 1656 (1972)

[12] D.I. Bonbright, R.G. Allas, R.O. Bondelid, E.L. Petersen, A.G. Pieper, R.B. Theus, I. Slaus, Phys. Rev.**C8**, 114 (1973)

[13] D.E. Gonzalez Trotter et al., ArXiv:nucl-ex/9904011v1 (1999)

[14] Cherubini S., Kondratyev V. N., Lattuada M., Spitaleri C., Miljanic D., Zadro M. and Baur G. ApJ **457**, 855 (1996)

[15] C. Spitaleri et al., Phys. Rev. **C60**, 055802 (1999)

[16] C. Spitaleri et al., Phys. Rev. **C69**, 055806 (2004)

[17] G. Calvi et al., Nucl. Phys. **A621**, 139c (1997)

[18] C. Spitaleri et al., Eur. Phys. J. **A7**, 181 (2000)

[19] M.A. Aliotta et al., Eur. Phys. J. **A9**, 435 (2000)

[20] M. Lattuada et al., Astrophys. J. **562**, 1076 (2001)

[21] A. Tumino et al., Nucl. Phys. **A718**, 449c (2003)

[22] A. Tumino et al., Phys. Rev. **C67**, 065803 (2003)

[23] M. Zadro et al., Phys. Rev. **C40**, 181 (1989)

[24] S. Romano et al., Nucl. Phys. **A738**, 406 (2004)

[25] N.S. Chant and P.G.Roos, Phys. Rev. **C15**, 57 (1977)

[26] U.G. Neudatchin and Y.F. Smirnov, At. Energy Rev. **3**, 157 (1965)

[27] G. Jacob and Th.A. Maris, Rev. Mod. Phys. **38**, 121 (1966)

[28] M. Jain, P.G.Roos, H.G.Pugh and H.D. Holgrem, Nucl. Phys **A153**, 49 (1970)

[29] P.G. Roos, N.S. Chant, D.A. Goldberg, H.D. Holdgren and R. Woody, Phys. Rev. **C15**, 69 (1977)

[30] M. La Cognata et al. Astrophys. J. **708**, 796 (2010)

[31] G.G. Ohlsen, Nucl. Inst. Meth. **37**, 240 (1965)

[32] A. Tumino et al., EPJ **A25**, 649 (2005)

[33] M. Gulino et al., LNS Act. Rep. **2**, 79 (2007)

[34] M. Gulino et al., LNS Act. Rep., 49 (2006)

[35] M. Gulino et al., Mem. SAIT, 481 (2007)

[36] J.C. Overley et al., Nucl. Phys. **A221**, 573 (1974)

[37] G. Baur, C.A. Bertulani, H. Rebel, Nucl. Phys. **A458**, 188 (1986)

[38] R.G. Pizzone et al. Phys. Rev. **C80**, 025807 (2009)

[39] R.G. Pizzone et al. Phys. Rev. **C71**, 058801 (2005)

[40] R.G. Pizzone et al. LNS Act. Rep., 41 **2** (2007)

[41] I. Tanihata et al. Phys. Rev. Lett. **55**, 2677 (1985)